tvst

Article

Microscope-Integrated OCT-Guided Volumetric Measurements of Subretinal Blebs Created by a Suprachoroidal Approach

Ananth Sastry[1], Jianwei D. Li[2], William Raynor[1], Christian Viehland[2], Zhenxi Song[2], Liangyu Xu[2], Sina Farsiu[2], Joseph A. Izatt[2], Cynthia A. Toth[1,2], and Lejla Vajzovic[1]

[1] Department of Ophthalmology, Duke University of School of Medicine, Durham, NC, USA
[2] Department of Biomedical Engineering, Duke University, Durham, NC, USA

Correspondence: Lejla Vajzovic, Department of Ophthalmology, Duke University School of Medicine, 2351 Erwin Road, Durham, 27710 NC, USA.
e-mail: lejla.vajzovic@duke.edu

Received: November 17, 2020
Accepted: April 6, 2021
Published: June 17, 2021

Keywords: subretinal bleb; subretinal delivery; microscope-integrated optical coherence tomography; suprachoroidal approach; image-guided surgery

Citation: Sastry A, Li JD, Raynor W, Viehland C, Song Z, Xu L, Farsiu S, Izatt JA, Toth CA, Vajzovic L. Microscope-integrated OCT-guided volumetric measurements of subretinal blebs created by a suprachoroidal approach. Transl Vis Sci Technol. 2021;10(7):24, https://doi.org/10.1167/tvst.10.7.24

Purpose: To investigate the use of imaging modalities in the volumetric measurement of the subretinal space and examine the volume of subretinal blebs created by a subretinal drug delivery device utilizing microscope-integrated optical coherence tomography (MIOCT).

Methods: An MIOCT image-based volume measurement method was developed and assessed for accuracy and reproducibility by imaging ceramic spheres of known size that were surgically implanted into ex vivo porcine eyes. This method was then used to measure subretinal blebs created in 10 porcine eyes by injection of balanced salt solution utilizing a subretinal delivery device via a suprachoroidal cannula. Bleb volumes obtained from MIOCT were compared to the intended injection volume.

Results: Validation of image-based volume measurements of ceramic spheres showed accuracy to $\pm$0.029 µL (5.6%) for objects imaged over the posterior pole and $\pm$0.025 µL (4.8%) over peripheral retina. The mean expected injection volume from extraocular tests of the suprachoroidal cannula was 66.44 µL ($\sigma = 2.4$ µL). The mean injection volume as measured by the MIOCT imaging method was 54.8 µL ($\sigma = 12.3$ µL), or 82.48% of expected injection volume.

Conclusions: MIOCT can measure the volume of subretinal blebs with accuracy and precision. The novel suprachoroidal approach using a subretinal delivery device was able to deliver greater than 80% of expected injection volume into the subretinal space, as assessed by MIOCT.

Translational Relevance: MIOCT provides a method for visualization, and analysis of images enables surgeons to quantify and evaluate the success of subretinal drug delivery via a suprachoroidal approach.

Introduction

Subretinal drug delivery is becoming an increasingly relevant and effective form of treatment for a variety of debilitating retinal diseases. This form of treatment first saw success in patients with the use of tissue plasminogen activator for massive submacular hemorrhages.[1] More recently, subretinal delivery of viral vectors as gene therapy has demonstrated efficacy and safety in treating heretofore untreatable retinal degenerations such as Leber's congenital amaurosis.[2,3] This form of subretinal gene therapy has also shown early signs of success with other inherited conditions such as choroideremia, achromatopsia, and retinitis pigmentosa.[4,5] Promising results have also been shown with subretinal delivery of retinal pigment epithelium stem cell scaffolds in patients with Stargardt's disease and advanced geographic atrophy in non-exudative age-related macular degeneration.[6–8] Despite these advances, there remain a number of important challenges and risks with the

current techniques of accessing the subretinal space. These challenges may limit the effectiveness of the new therapeutics intended for subretinal delivery.

The current surgical paradigm of accessing the subretinal space for drug delivery involves performing a pars plana vitrectomy and a retinotomy, usually with a 38- or 41-gauge needle.[9] A subretinal bleb is then created as the drug is injected into the subretinal space. This technique has been further refined with the use of spectral-domain intraoperative optical coherence tomography (iOCT), which may facilitate the surgeon's view of the subretinal space.[9,10]

Direct, real-time visualization of the subretinal space with assessment of instrument depth remains a challenge even with the use of current, commercially available spectral-domain iOCT systems due to shadowing artifacts on the OCT created by standard intraocular surgical instruments.[11] Incorrect assessment of depth can lead to complications such iatrogenic penetration of Bruch's membrane, choroidal rupture, retinal detachment, or inadvertent injection of the medication into the vitreous cavity or suprachoroidal space.[12]

The creation of a retinotomy can increase the risk of developing proliferative vitreoretinopathy and visual field defects.[13] The risk of proliferative vitreoretinopathy or vitritis may be exacerbated by inadvertent reflux of stem cells or viral vectors into the vitreous cavity.[5] These challenges are further compounded when performing this technique in pediatric patients, which have become the target population for early intervention with subretinal gene therapy. Performing a pars plana vitrectomy in pediatric patients can be technically difficult due to dense vitreoretinal adhesions and risk of causing a retinal break when inducing a posterior vitreous detachment.[14]

Alternative methods of accessing the subretinal space have been investigated. Ho et al.[15] examined the use of subretinal stem-cell delivery utilizing a subretinal ab externo device (iTrack microcatheter; Nova Eye Medical, Fremont, CA), which involved a peripheral sclerotomy and choroidal fistula to attain subretinal cannulation using a beacon tip to determine the location of the device. The study demonstrated an unacceptably high rate of adverse events with the use of this technique; adverse events occurred in 97.1% of surgical subjects, 58% of which were related to the surgical delivery system, including retinal perforation and retinal detachment. Subsequently, a subretinal delivery device that utilizes the suprachoroidal space was developed to avoid the complications related to retinotomy and subretinal cannulation. This device involved a microcannula that passes through the suprachoroidal space via a sclerotomy toward the posterior pole under microscopic visualization. Once in the desired position, an internal 35-gauge needle within the cannula is deployed through the choroid and Bruch's membrane and into the subretinal space. Experiments in a preclinical model demonstrated feasibility of subretinal drug delivery using this device.[16] A recent follow-up phase 2b study by Heier et al.[17] evaluated the safety of this device in the delivery of subretinal stem cells in 21 patients. Cells were delivered to the subretinal space successfully in 86% of participants. Although significant loss of vision was reported in the operative eye in 14.3% of participants for unknown reasons, there were no cases of endophthalmitis, retinal detachment, significant choroidal hemorrhage, retinal perforation, cell egress, or need for unplanned vitrectomy.

Finally, with any approach to the subretinal space, there remains a nebulous relationship between the intended volume of subretinal drug delivery and the volume that is actually delivered to the subretinal space. Although the surgeon is able to see the generation of a subretinal bleb from the en face view and with the assistance of iOCT, there is no method to determine the percentage of volume delivery, and any assessment of a successful bleb is based on estimation. This problem is clinically significant, as any volume inadvertently delivered outside of the subretinal space creates a dose discrepancy, which may translate to reduced viral transduction of target cells and potentially result in a suboptimal therapeutic effect, particularly for treatments that require dose escalation.[5] Hsu et al.[18] sought to address this question by obtaining measurements of subretinal bleb volumes using swept-source microscope-integrated OCT (MIOCT) imaging in porcine eyes. Utilizing a high-magnification contact lens viewing system in conjunction with MIOCT, the authors were able to accurately calculate the volume of subretinal blebs in an ex vivo porcine model. While creating subretinal blebs using the standard vitrectomy/retinotomy technique, reflux of the injected fluid into the vitreous cavity was observed by the surgeon in 64% (seven out of 11) of cases. In the remaining four eyes where no leakage was observed by the surgeon, the mean delivered volume was 32 µL, which is 64% of the 50 µL intended volume. The mean MIOCT-measured loss of the intended injection in these eyes was 36%, ranging between 12% and 73%.

Due to the challenges associated with subretinal drug delivery and concurrent intraoperative imaging techniques, we aimed to improve on methods that utilize intraoperative OCT imaging to measure the volume of subretinal blebs, including the use of a viewing system with a wider field of view in order to capture larger or more peripheral blebs. In addition, we sought to evaluate the ability of MIOCT to

measure the volume of subretinal blebs created by the novel suprachoroidal approach. We hypothesized that volumes of subretinal blebs created by a suprachoroidal approach could be measured accurately and precisely using our improved measurement techniques based on MIOCT images. We further postulated that volumetric measurements of subretinal bleb volume would be feasible using a viewing system with a wider field of view than that of a high magnification contact lens. Finally, we aimed to achieve less than 20% loss of subretinal volume delivery relative to intended volume delivery using the suprachoroidal approach for injection.

Methods

In this study, we utilized a swept-source MIOCT prototype system developed at Duke University to image subretinal blebs that were created in an ex vivo porcine animal model.[19] The Duke MIOCT system is a 100-kHz swept-source OCT system at 1050 nm. Fast imaging speeds and a high signal-to-noise ratio enabled by a swept-source system enable greater visualization of surgical maneuvers. An electrically tunable lens allowed for dynamic focus adjustment, ensuring that the OCT system was parfocal with the surgical microscope.[20] We acquired volumetric images with 1000 A-scans/B-scan and 1000 B-scans/volume through a wide-angle contact lens (Mini Quad; Volk Optical, Inc., Mentor, OH). To ensure that the MIOCT system was capable of measuring bleb volume with accuracy and precision, it was first tested on objects with known volumes. A validation model similar to the one devised in the study by Hsu et al.[18] was used for this purpose.

Validation Model

Pars plana vitrectomies were performed in ex vivo porcine eyes. White ceramic alumina spheres 1 mm in diameter were surgically inserted into the vitreous cavities of the porcine eyes via a sclerotomy created by an MVR blade (Fig. 1A). OCT images of the spheres (Fig. 1B) were then captured through the wide-angle contact lens that had been placed on the cornea. Ceramic spheres were chosen as they had been previously shown to produce high-quality images on OCT. Although the bottom half of the spheres cannot be easily imaged due to shadowing artifact, the top half of the spheres can be imaged clearly with very distinct edges (Figs. 1C, 1D). The resulting hemispherical image provided an excellent surrogate for subretinal

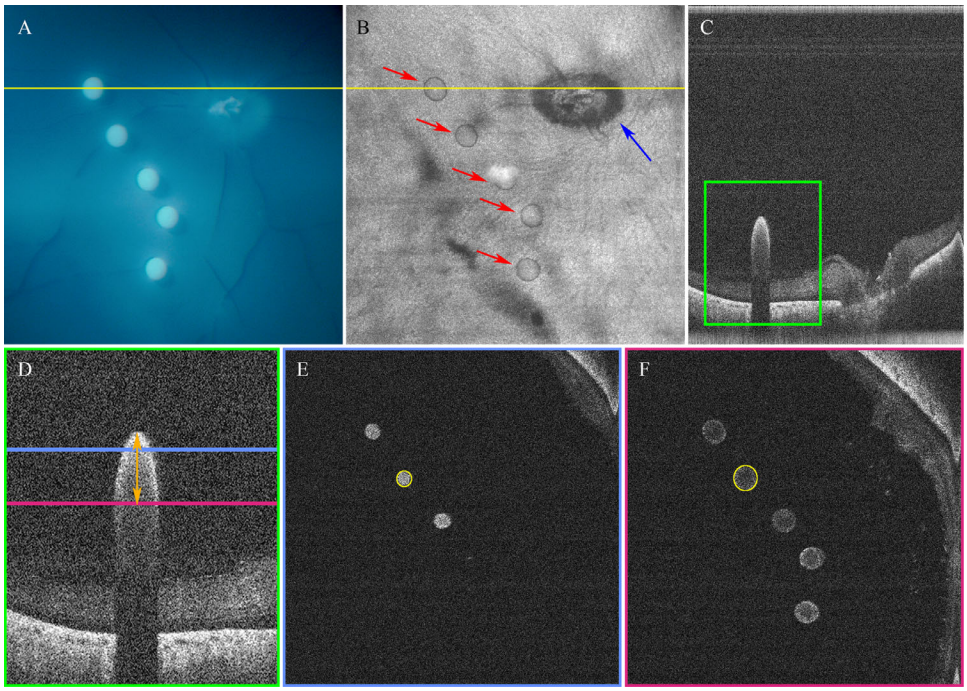

Figure 1. (A) Surgeon's view of ceramic spheres in vitreous cavity overlying posterior pole. (B) En face OCT imaging of the same ceramic spheres (*red arrows*) adjacent to the optic nerve (*blue arrow*). (C) B-scan cross-sectional image (*yellow line*) of ceramic sphere. (D) Magnified view of C; the entire sphere cannot be imaged due to shadowing artifact, but the upper half of the ceramic sphere can be visualized (*orange double-arrow*). (E, F) En face OCT image near the top of the sphere (*light blue line* from 1D) and at the equator of the sphere (*light red line* from D), respectively. The *yellow circle* indicates the manual segmentation used to calculate the sphere volume.

Table 1. Calibration Measurements

	Central Spheres ($n = 57$)	Peripheral Spheres ($n = 15$)
Human eye model calculated volume	0.819 +/− 0.046 µL	0.847 +/− 0.041 µL
Actual volume	0.524 µL	0.524 µL
Volume calibration factor	0.639	0.619
Standard deviation	0.029 µL (5.6%)	0.025 µL (4.8%)

blebs, which have a similar shape and appearance on OCT imaging. The diameters of the spheres were noted to be 1 mm in diameter by the manufacturer. This was confirmed using electronic calipers and resulted in a calculated spherical volume of 0.524 µL.

The en face images (Fig. 1) generated of each sphere were manually segmented by tracing the boundaries of the top hemisphere using ImageJ (National Institutes of Health, Bethesda, MD). To ensure reproducibility between each scan, the lower boundary was always set as the equator of the sphere. Because the Z-pitch of pixels is an inherent property of the swept-source laser clock and digitizer, any errors in accuracy are negligible compared to segmentation error. The Z-pitch is used to convert the known length of the radius of the sphere into pixels, a value that is then used to calculate the location of the equator at the z-axis as a fixed number of pixels drawn down from the top of the sphere (Fig. 1D). A lens reflection artifact in the image was used as a fiducial marker to calibrate an optical model of the OCT scanner and eye and subsequently determine the X- and Y-pitch at every pixel in the en face image. The X-, Y-, and Z-pitches were multiplied to determine the volume of every voxel (a cuboid on a three-dimensional grid) in the acquired OCT scan. All of the segmented voxels from the segmented en face images were summed to determine the volume of the hemisphere and then doubled to get the full spherical volume. This was performed 57 times for spheres placed in a central location in the vitreous cavity and 15 times for spheres placed in a more peripheral portion of the widefield viewing system. The mean calculated volume and corresponding standard deviation were obtained for spheres in the central location and in the peripheral location. This was compared to the actual volume of the sphere to develop a volume calibration factor that was found to result in accurate and precise measurements (Table 1).

Measurement of Subretinal Blebs Based on MIOCT Measurements

Subretinal Injection Device

A subretinal drug delivery device (Orbit Subretinal Delivery System [SDS]; Gyroscope Therapeutics Ltd., Stevenage, UK) (Fig. 2) that utilizes a novel suprachoroidal approach to access the subretinal space was used to create subretinal blebs in 37 ex vivo porcine eyes, each of which was individually numbered from 1 to 37. The device consists of a long cannula that is connected to a 1-cc syringe and dose-clip. The device has two fluid lines labeled "BSS" (balanced salt solution) and "Dose," allowing for independent injection of BSS for an entry bleb followed by a controlled dose volume. The handpiece can be secured to a third-arm apparatus that attaches to the surgeon's wrist rest.

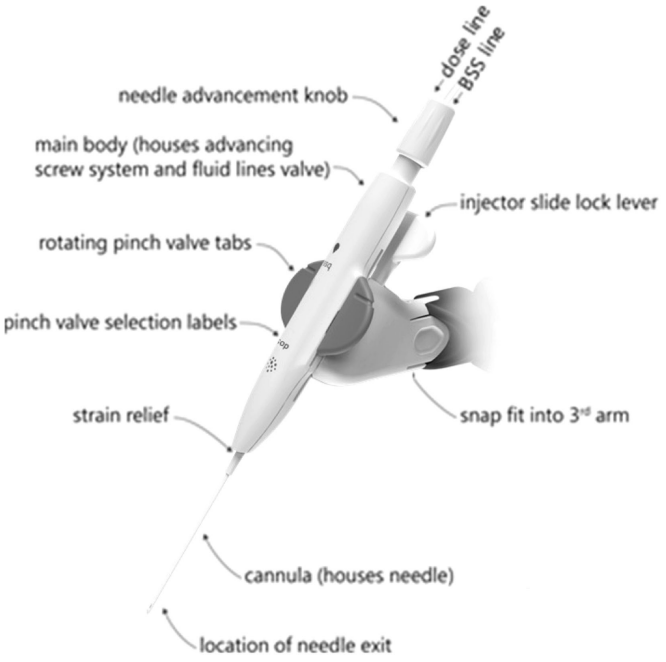

Figure 2. Schematic of the Orbit SDS.

In order to determine the intended injection volume, the device and syringe were filled and primed with BSS. The dose clip was removed, and the full injection was delivered onto a mass scale 10 separate times. Each of these masses was recorded. This process was repeated again with another copy of the device and syringe to provide another 10 measurements. Given that the density of BSS approximates that of water (1 g/cm^3) with negligible differences, each mass measurement in milligrams was recorded as the volume in microliters (Table 2).

Table 2. Volume Injected by Subretinal Injection Devices

Device 1		Device 2	
Measurement #	Volume (µL)	Measurement #	Volume (µL)
1	67.6	1	66.5
2	66.4	2	67.5
3	66.6	3	67.1
4	64.9	4	67.3
5	68.3	5	66.0
6	66.2	6	68.7
7	65.9	7	66.8
8	67.5	8	65.9
9	68.7	9	66.7
10	56.8	10	67.3

Mean injected volume for devices 1 and 2 was 66.44 µL (SD = 2.4 µL).

Surgical Technique

Non-vitrectomized, ex vivo porcine eyes were placed into a plastic model orbit and fixed into place using a metal clip on the optic nerve. An intraocular chandelier was placed into the superonasal quadrant using a 25-gauge trocar and cannula. A peritomy was then performed on the temporal side to expose the sclera. A marking pen was used to place ink on the ophthalmic marker (Orbit Biomedical, Ambler, PA), which was then used to create two marks on the bare temporal sclera parallel to the limbus 3 mm apart and 6 mm posterior to the limbus. A crescent blade was then used to create a 3-mm incision parallel to the limbus and perpendicular to the sclera down to the suprachoroidal space between the two marked points. Next, the syringe and device were filled with BSS and primed. The device was then attached to the third arm, which was affixed to the temporal portion of the wrist rest such that the cannula was aimed posteriorly at the temporal surface of the globe.

At this point, the chandelier was turned on and a Leica M840 operating microscope (Leica Camera AG, Wetzlar, Germany) with MIOCT and the NGENUITY 3D Visualization System (Alcon, Fort Worth, TX) was brought into the field. The widefield lens was placed onto the cornea. Next, the Orbit SDS cannula was inserted through the sclerotomy and advanced through the suprachoroidal space toward the posterior pole. The location of the cannula edge could be visualized internally using the NGENUITY 3D Visualization System (Fig. 3). When the tip of the cannula was found to be in a desirable location, the MIOCT system was turned on and centered over the raised edge of the cannula tip. The needle was then deployed until it was observed with the NGENUITY 3D Visualization System to be in the subretinal space. A small volume of fluid was then injected to generate a small entry bleb in order to confirm that the needle tip was in the correct space. The creation of the bleb was viewed both under direct visualization with widefield imaging and with the use of the MIOCT B-scan and en face view (Fig. 4). A full OCT scan (nominally 18.1 mm × 17.8 mm) of the entry bleb was then captured and saved. The fluid line was switched to "Dose"; the dose clip was removed, and the plunger was fully depressed. Upon creation of the full bleb, the needle was retracted, and the cannula was removed. An OCT scan of the full bleb (Fig. 5) was then captured and saved.

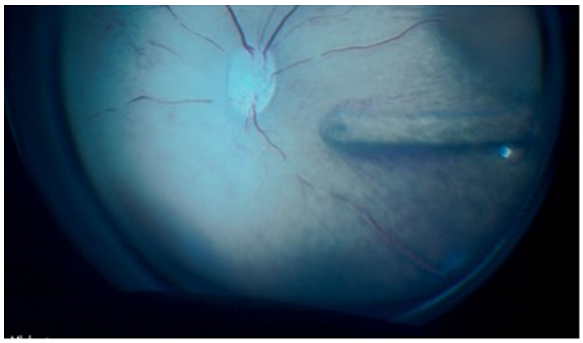

Figure 3. Orbit SDS flexible cannula is threaded in the suprachoroidal space toward the posterior pole. The surgeon is able to directly visualize the cannula using the NGENUITY 3D Visualization System with chandelier endoillumination.

Image Processing

Of the 37 porcine eyes that were prepped, seven were screened out before a bleb was created due to tissue damage that occurred when attempting to pass the cannula through dense suprachoroidal adhesions or when the needle was passed through the retina. This

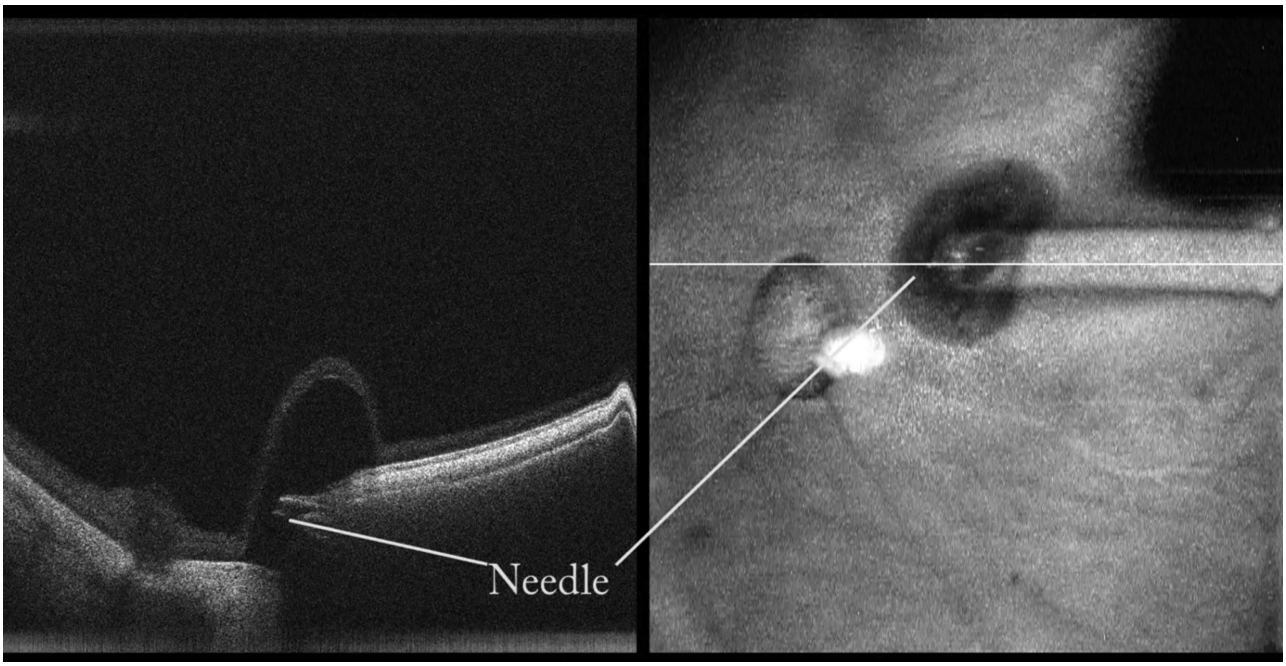

Figure 4. Entry bleb captured intraoperatively by MIOCT with the B-scan (*left panel*) and en face (*right panel*) view. In the B-scan view, the position of the cannula is noted by the sub-retinal pigment epithelium (RPE) elevation seen on the right side of the bleb. The needle tip can also be visualized in both viewing systems.

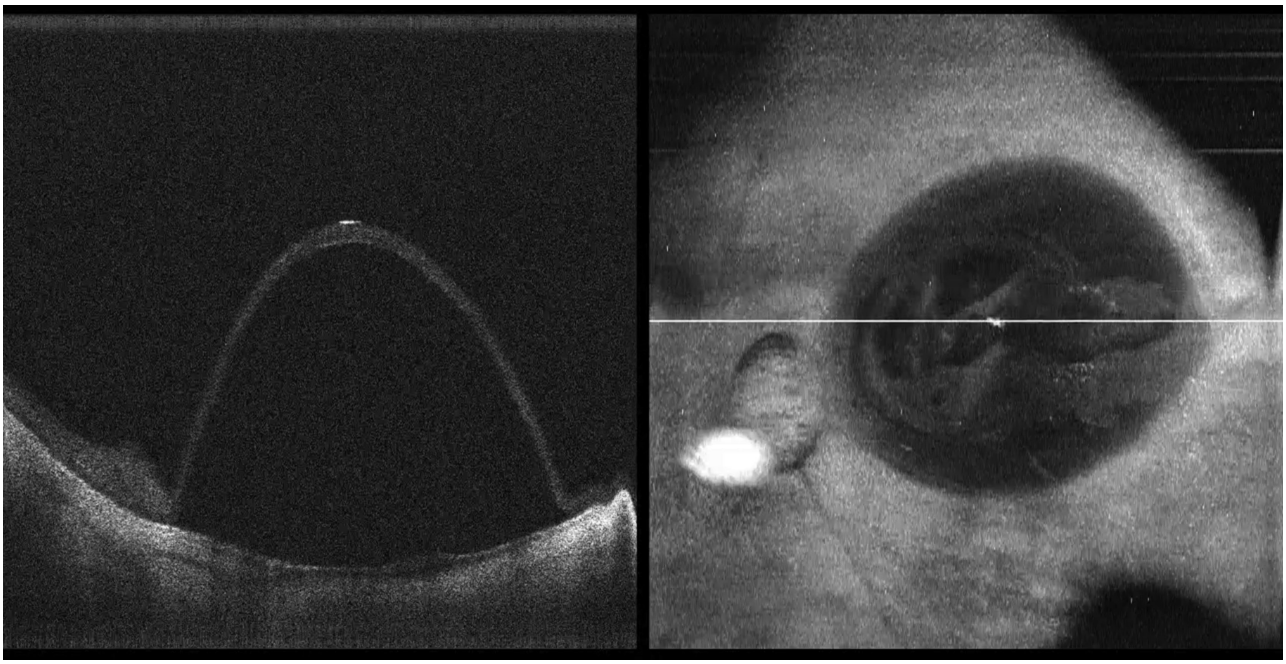

Figure 5. Full/complete bleb captured with MIOCT. B-scan view (*left panel*) and en-face view (*right panel*).

technique is counter to surgical guidance in human cases, where surgeons are directed to not advance further if they encounter resistance; the aggressive technique was performed to ensure blebs were posterior enough to be properly visualized by MIOCT. Of the remaining 30 eyes for which a subretinal bleb was successfully created, an OCT volume scan was successfully captured and saved for 26 eyes. The OCT images from the 26 eyes were graded by one grader (JL) on a scale for image quality using a composite

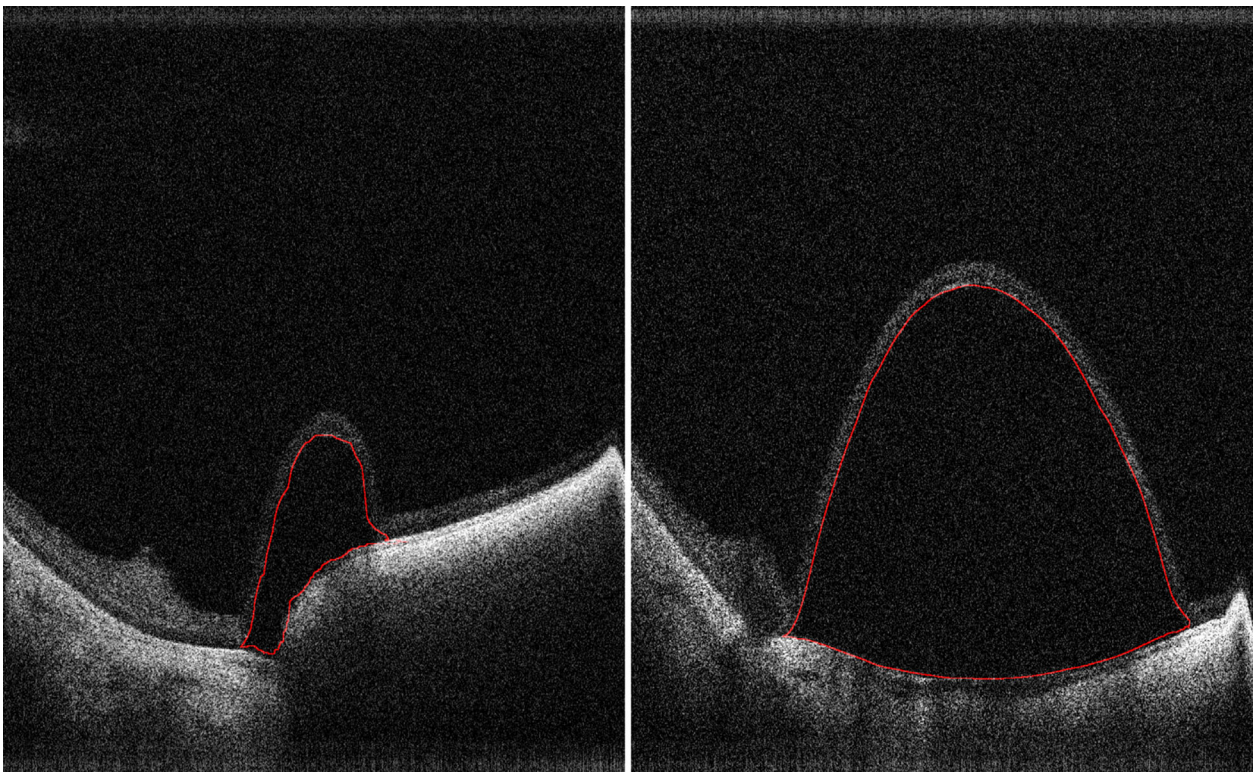

Figure 6. Subretinal blebs after manual segmentation. (*Left panel*) Entry bleb. (*Right panel*) Full bleb (*red* indicates traced boundary).

score based on the following criteria: presence of air bubbles, which would negatively affect visibility of the bleb; presence of a lens reflection artifact required to perform calibrated quantitative measurements; lateral visibility of bleb; and visibility of the top and bottom boundaries of the bleb. Each factor was considered to be equally important, and numeric scores were assigned to each category, where higher numbers indicated a more desirable outcome. These scores were applied to both entry and full blebs, and the scores for the two blebs for each eye were combined via a weighted average. Review of the 26 eyes by the grader found two eyes without the lens artifact necessary to calculate volume and one eye with abnormally decreased resolution. The eyes with the top 10 composite scores out of the remaining 23 eyes were selected for manual segmentation. The 1000 B-scans for each entry and full bleb for each of these 10 eyes were averaged into 250 B-scans. Each B-scan was then manually segmented using Duke Optical Coherence Tomography Retinal Analysis Program (DOCTRAP) software (Fig. 6).[21] The volumes of each entry and full bleb were subsequently determined using the method described above in the "validation" section. The entry bleb volumes were subtracted from the corresponding full bleb volumes to determine the final volume for each bleb.

Statistical Analysis

The calibration uncertainty factor was determined by the standard deviation of the volume from the calibration model. The segmentation uncertainty was determined by estimating an approximately 5-pixel range of potential bias, which could either expand or shrink the segmented area. A Monte Carlo simulation was run to estimate the volume error. The total measurement uncertainty was calculated by taking the square root of the sum of the squares of the calibration uncertainty and segmentation uncertainty. The mean image-based volume of the subretinal blebs from injections was compared to the mean intended injection volume using absolute difference and percent error.

Results

Validation of MIOCT Image-Based Volume Measurements

The calculated volume of the ceramic sphere was found to be 0.819 ± 0.046 µL for central spheres and 0.847 ± 0.041 µL for peripheral spheres (Table 1). This was compared to the actual volume of 0.524 µL,

which resulted in calibration factors of 0.639 and 0.619, respectively. The standard deviation was found to be approximately 0.029 µL (5.6%) for central spheres and 0.025 µL (4.8%) for the peripheral spheres. Using a 5-pixel range of potential bias, the Monte Carlo simulation found a ±4.8% segmentation uncertainty error. Thus,

$$\text{Total uncertainty} = \sqrt{\text{Calibration uncertainty}^2 + \text{Segmentation uncertainty}^2}$$

$$= \sqrt{4.8^2 + 4.8^2} = 6.8\%$$

Measurement of Subretinal Bleb Volumes Based on MIOCT Images

The mean control volume injected for devices 1 and 2 was found to be 66.44 ± 2.4 µL (Table 2). The mean entry bleb volume was found to be 5.14 ± 1.68 µL. The mean subretinal bleb volume (full bleb volume minus entry bleb volume) was found to be 54.8 ± 12.3 µL (Table 3). The minimum, median, and maximum subretinal bleb volumes were 32.8 µL, 57.45 µL, and 69.6 µL, respectively. Figure 7 shows a graphic representation of the calculated subretinal bleb volume of each of the 10 eyes with the top composite scores (numbers 8, 21, 23, 24, 26, 29, 30, 31, and 37) compared against the mean calculated volume.

The mean subretinal bleb volume was 82% of the mean intended injection volume. In seven of the 10 eyes, the bleb achieved 80% or greater of the mean intended volume. The mean percent error of the mean measured volume relative to the mean intended volume was 18%. Comparing the minimum, median, and maximum subretinal bleb volumes against the mean intended volume yielded maximum, median, and minimum percent errors of 50%, 14%, and 1%, respectively.

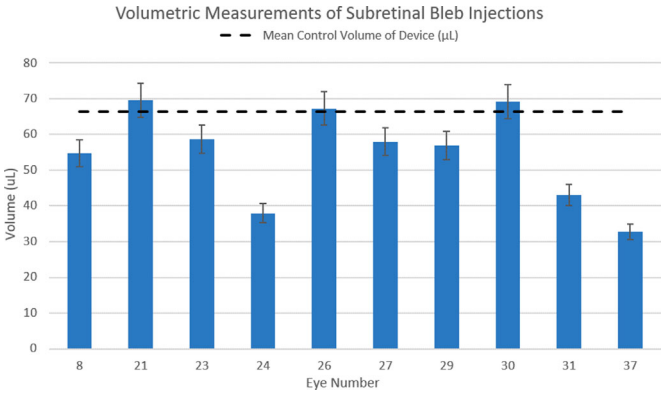

Figure 7. Subretinal bleb volume measurements. Error bars illustrate the range of calculated uncertainty error for segmentation (6.8%). Volumes are compared against the mean control volume of the device (*dashed line*).

In three of the 10 eyes (24, 31, and 37), the volume loss appeared to be most pronounced (Fig. 7). MIOCT images and scans for these eyes at each step of the procedure were analyzed post hoc by four reviewers (AS, JL, WR, LV) to determine a possible cause for the larger fluid loss. The reviewers did not find a single imaging or intraoperative finding that was consistent among all three eyes to conclusively explain the pronounced volume loss.

Discussion

In this study, we attempted to address a number of the limitations of the current paradigm of subretinal drug delivery. We first replicated the method described by Hsu et al.[18] used to validate the ability for the MIOCT to calculate the volume of particular intraocular objects. Using the calibration factor that

Table 3. Subretinal Bleb Volume Measurements

Eye	Eye Length (mm)	Entry Volume (µL)	Final Volume (µL)	Injected Volume (µL)
8	28.0	7.00	61.7	54.7
21	27.8	7.21	76.8	69.6
23	27.4	2.33	61.1	58.7
24	27.6	7.79	45.8	38.0
26	27.7	4.84	72.2	67.3
27	28.3	4.34	62.3	58.0
29	28.0	3.47	60.4	56.9
30	28.3	5.32	74.5	69.2
31	28.4	5.31	48.4	43.1
37	27.0	3.77	36.6	32.8
Mean ± SD	27.9 ± 0.420	5.14 ± 1.68	60.0 ± 12.4	54.8 ± 12.3

was ascertained from this method, we were able to reliably measure the volume of the ceramic sphere with precision and accuracy with no more than a 5.6% error rate. This supports the previous study, which was able to reliably measure volume of known objects within 6% of actual volume. Our data add to the previous study by demonstrating that this method can also be used with a widefield viewing lens, as the prior study used a high-magnification contact lens. The widefield viewing lens also allowed us to compare the accuracy in measurement of spheres in the center of the field against spheres imaged in the peripheral portion of the field. Interestingly, there was a negligible difference in the calibration factors between these two groups (0.639 and 0.619, respectively). It was also interesting to note that the percent error was actually somewhat lower for the peripheral spheres (4.8%) compared with the central spheres (5.6%).

Next, we assessed the use of MIOCT in conjunction with the novel subretinal drug delivery device. Unlike in humans, porcine anatomy provides challenges to instrumentation in the suprachoroidal space. Tight junctions exist between the sclera and choroid in the area centralis of porcine eyes.[22] In order to reach a posterior bleb site that could be fully visualized by MIOCT, a more aggressive technique of forcefully dissecting past adhesions with the cannula was adopted. These technique modifications allowed for improved bleb placement but resulted in seven eyes being screened out due to technique-related tissue damage. Choroidal damage and retinal perforations were not observed when using the unmodified technique in the previously mentioned human safety study.[17] The design of the Orbit SDS provided ergonomic ease of cannula manipulation for the surgeon. The third arm, which held the device in place, provided stability for the surgeon and further facilitated instrument maneuvers. The use of the MIOCT and the NGENUITY 3D Visualization System in conjunction with the Orbit SDS allowed for direct visualization of the cannula and needle tip into the subretinal space using multiple visual cues.

Finally, we attempted to see if subretinal bleb volumes could be measured in the context of the suprachoroidal approach to subretinal injection. We found that subretinal blebs of sufficient image quality could be measured adequately when created by a suprachoroidal approach. With this approach, there was a mean volume loss of 18%, which achieved the goal of less than 20% loss of subretinal volume delivery relative to intended volume delivery. Additionally, seven of the 10 eyes achieved a volume delivery of greater than 80% relative to the mean intended volume. Three of the 10 eyes had pronounced volume loss relative to mean intended volume. Post hoc review of all MIOCT images for these three did not demonstrate a common pattern or finding to explain the difference between these eyes and the other seven. However, because we did not notice obvious leakage into the vitreous cavity during the procedures in these 10 eyes, we suspect that the bleb volume loss may have been reflux of fluid into the suprachoroidal space. Overall, this suggests an improvement over the standard transvitreal approach in regard to percentage of volume delivered as assessed by MIOCT and as compared to prior study by Hsu et al.[18] Further study with direct comparison of two delivery methods would be indicated.

Our study had a number of weaknesses and limitations. First, there was a selection bias in that only the eyes with image qualities sufficient for adequate and reliable segmentation were chosen for image processing and volume calculation. Eyes with lower OCT image quality, eyes with tissue damage from the modified technique, and those with intra-bleb air bubbles were excluded from the dataset, as these could lead to potentially inaccurate volume calculations. Second, our study used BSS as the subretinal fluid injectate, which is transparent and therefore of limited utility when trying to assess for occult leaks. The use of diluted triamcinolone acetonide, which was used by Hsu et al.[18] may have allowed the authors to rule out retinal perforations and leaks into the vitreous cavity. However, in this study, triamcinolone acetonide was not used because it was observed to settle out of solution in the syringe before injection. Finally, our study was conducted in porcine eyes, which have various biomechanical differences compared with human eyes, such as the presence of dense chorioscleral adhesions. Additional research in ex vivo human eyes might be useful to assess the feasibility of this device.

Our study does lend itself to numerous interesting questions and future experiments. Our data cannot be directly compared to the data/outcomes found by Hsu et al.,[18] as different imaging modalities were used in each study. An experiment directly comparing the volume of subretinal blebs created by the transretinal approach against the suprachoroidal approach under the same conditions and parameters in ex vivo human eyes could provide very useful insights regarding the possible superiority of one technique over the other and could potentially change our current surgical paradigm. Similarly, comparing volumes of subretinal blebs created with and without the use of MIOCT assistance could address questions regarding the utility of intraoperative imaging with particular surgical techniques. The examination of other factors such as the relationship between intraocular pressure and the volume of drug delivery may lead to insights

regarding the cause of reflux of the subretinal injectate into the vitreous cavity or deep structures of the eye. Finally, manual segmentation of each individual B-scan for a given subretinal bleb is both time consuming and impractical for clinical use. The development of an automated segmentation algorithm to instantaneously segment and calculate the volume of subretinal blebs would allow for nearly real-time volume analysis and provide data for intraoperative surgeon feedback.[23] This may be valuable to future gene and stem cell therapy.

Conclusions

MIOCT can be used to measure the volume of central or peripheral subretinal blebs with accuracy and precision under high-magnification or widefield viewing systems. It provides a method for visualization and quantification of subretinal drug delivery and enables surgeons to evaluate the success of subretinal drug delivery performed by the novel suprachoroidal approach using the Orbit SDS. The suprachoroidal approach was able to deliver a mean of 80% of intended injection volume to the subretinal space. The combined use of MIOCT with a delivery system that enables access to the subretinal space without vitrectomy may improve subretinal therapy delivery and, therefore, treatment efficacy.

Acknowledgments

Supported by Orbit Biomedical (now part of Gyroscope Therapeutics), as well as by grants from the VitreoRetinal Surgery Foundation and the National Institutes of Health (U01 EY028079, R01 EY023039). Orbit Biomedical and Volk provided research equipment for the study and technical support in use of the device.

Disclosure: **A. Sastry**, None; **J.D. Li**, None; **W. Raynor**, None; **C. Viehland**, None; **Z. Song**, None; **L. Xu**, None; **S. Farsiu**, None; **J.A. Izatt**, Leica Microsystems (P, F), Carl Zeiss Meditec (P, F), St. Jude Medical Center (P, F); **C.A. Toth**, Alcon (F), Hemosonics (F), Emmes (C); **L. Vajzovic**, Orbit Biomedical (C), Alcon (C), Alimera Sciences (C), Allergan (C), Aerie (C), Bausch + Lomb (C), DORC (C), Guidepoint (C), Roche/Genentech (C), Second Sight (C), Evolve Medical Education (C)

References

1. Peyman GA, Nelson NC, Jr, Alturki W, et al. Tissue plasminogen activating factor assisted removal of subretinal hemorrhage. *Ophthalmic Surg*. 1991;22(10):575–582.
2. Maguire AM, High KA, Auricchio A, et al. Age-dependent effects of RPE65 gene therapy for Leber's congenital amaurosis: a phase 1 dose-escalation trial. *Lancet*. 2009;374(9701):1597–1605.
3. Russell S, Bennett J, Wellman JA, et al. Efficacy and safety of voretigene neparvovec (AAV2-hRPE65v2) in patients with RPE65-mediated inherited retinal dystrophy: a randomised, controlled, open-label, phase 3 trial. *Lancet*. 2017;390(10097):849–860.
4. Ghazi NG, Abboud EB, Nowilaty SR, et al. Treatment of retinitis pigmentosa due to MERTK mutations by ocular subretinal injection of adeno-associated virus gene vector: results of a phase I trial. *Hum Genet*. 2016;135(3):327–343.
5. Xue K, Groppe M, Salvetti AP, MacLaren RE. Technique of retinal gene therapy: delivery of viral vector into the subretinal space. *Eye (Lond)*. 2017;31(9):1308–1316.
6. Kashani AH, Lebkowski JS, Rahhal FM, et al. A bioengineered retinal pigment epithelial monolayer for advanced, dry age-related macular degeneration. *Sci Transl Med*. 2018;10(435):eaao4097.
7. Schwartz SD, Hubschman J-P, Heilwell G, et al. Embryonic stem cell trials for macular degeneration: a preliminary report. *Lancet*. 2012;379(9817):713–720.
8. Schwartz SD, Tan G, Hosseini H, Nagiel A. Subretinal transplantation of embryonic stem cell-derived retinal pigment epithelium for the treatment of macular degeneration: an assessment at 4 years. *Invest Ophthalmol Vis Sci*. 2016;57(5):ORSFc1–ORSFc9.
9. Davis JL, Gregori NZ, MacLaren RE, Lam BL. Surgical technique for subretinal gene therapy in humans with inherited retinal degeneration. *Retina*. 2019;39(suppl 1):S2–S8.
10. Ehlers JP, Petkovsek DS, Yuan A, Singh RP, Srivastava SK. Intrasurgical assessment of subretinal tPA injection for submacular hemorrhage in the PIONEER study utilizing intraoperative OCT. *Ophthalmic Surg Lasers Imaging Retina*. 2015;46(3):327–332.
11. Ehlers JP, Tao YK, Farsiu S, Maldonado R, Izatt JA, Toth CA. Integration of a spectral domain

optical coherence tomography system into a surgical microscope for intraoperative imaging. *Invest Ophthalmol Vis Sci.* 2011;52(6):3153–3159.
12. Westenskow PD, Kurihara T, Bravo S, et al. Performing subretinal injections in rodents to deliver retinal pigment epithelium cells in suspension. *J Vis Exp*. 2015;(95):52247.
13. McDonald HR, Lewis H, Aaberg TM, Abrams GW. Complications of endodrainage retinotomies created during vitreous surgery for complicated retinal detachment. *Ophthalmology*. 1989;96(3):358–363.
14. Rejdak R, Nowakowska D, Wrona K, Maciejewski R, Junemann AG, Nowomiejska K. Outcomes of vitrectomy in pediatric retinal detachment with proliferative vitreoretinopathy. *J Ophthalmol*. 2017;2017:8109390.
15. Ho AC, Chang TS, Samuel M, Williamson P, Willenbucher RF. Experience with a subretinal cell-based therapy in patients with geographic atrophy secondary to age-related macular degeneration. *Am J Ophthalmol*. 2017;179:67–80.
16. Baldassarre JS, Joseph A, Keane M, Heier JS. Subretinal delivery of cells via the suprachoroidal space: Janssen trial. In: Schwartz SD, Nagiel A, Lanza R, eds. *Cellular Therapies for Retinal Disease: A Strategic Approach*. Cham, Switzerland: Springer International Publishing; 2017.
17. Heier JS, Ho AC, Samuel MA, et al. Safety and efficacy of subretinally administered palucorcel for geographic atrophy of age-related macular degeneration: phase 2b study. *Ophthalmol Retina*. 2020;4(4):384–393.
18. Hsu ST, Gabr H, Viehland C, et al. Volumetric measurement of subretinal blebs using microscope-integrated optical coherence tomography. *Transl Vis Sci Technol.* 2018;7(2):19.
19. Carrasco-Zevallos OM, Keller B, Viehland C, et al. Live volumetric (4D) visualization and guidance of in vivo human ophthalmic surgery with intraoperative optical coherence tomography. *Sci Rep*. 2016;6:31689.
20. Tao YK, Srivastava SK, Ehlers JP. Microscope-integrated intraoperative OCT with electrically tunable focus and heads-up display for imaging of ophthalmic surgical maneuvers. *Biomed Opt Express*. 2014;5(6):1877–1885.
21. Chiu SJ, Li XT, Nicholas P, Toth CA, Izatt JA, Farsiu S. Automatic segmentation of seven retinal layers in SDOCT images congruent with expert manual segmentation. *Opt Express*. 2010;18(18):19413–19428.
22. Olsen TW, Feng X, Wabner K, et al. Cannulation of the suprachoroidal space: a novel drug delivery methodology to the posterior segment. *Am J Ophthalmol*. 2006;142(5):777–787.
23. Song Z, Xu L, Wang J, et al. Lightweight learning-based automatic segmentation of subretinal blebs on microscope-integrated optical coherence tomography images. *Am J Ophthalmol*. 2021;221:154–168.